The Astrophysical Journal Supplement Series, 164:536–551, 2006 June
© 2006. The American Astronomical Society. All rights reserved. Printed in U.S.A.

A COMPARATIVE STUDY OF ION CHARACTERISTICS IN THE LARGE GRADUAL SOLAR ENERGETIC PARTICLE EVENTS OF 2002 APRIL 21 AND 2002 AUGUST 24

A. J. Tylka,[1] C. M. S. Cohen,[2] W. F. Dietrich,[3,1] M. A. Lee,[4] C. G. Maclennan,[5]
R. A. Mewaldt,[2] C. K. Ng,[6,7] and D. V. Reames[6]
Received 2005 September 21; accepted 2006 January 25

ABSTRACT

Solar energetic particles (SEPs) provide an opportunity to study in detail the processes of particle acceleration and transport that are ubiquitous in astrophysical plasmas. Tylka et al. focused on the problem of SEP spectral and compositional variability at energies above a few tens of MeV per nucleon. They motivated their study with two large, gradual SEP events, 2002 April 21 and 2002 August 24, which have similar fast coronal mass ejections (CMEs) and flares but nevertheless illustrate the extremes of high-energy behavior. In this paper, we present additional detailed comparisons between the ion characteristics of these events. These results should be helpful in developing and testing new SEP models, which are currently under development.

Subject headings: acceleration of particles — shock waves — Sun: coronal mass ejections (CMEs) — Sun: flares — Sun: particle emission

1. INTRODUCTION

One advantage in studying solar energetic particles (SEPs) is the detailed nature of the observations available to us. These observations include characteristics of the flares and coronal mass ejections (CMEs) that initiate the SEP event, the concomitant interplanetary conditions (at least near Earth), and in situ particle measurements over a wide range of species and energies. Minor heavy ions (with atomic number $Z > 2$) are particularly useful in this regard: they are genuine "test particles," too few in number to generate a feedback effect on the acceleration and transport processes. These minor ions also have various charge-to-mass (Q/A) ratios, which serve to identify seed populations and to probe the velocity- and rigidity-dependent effects that govern injection, acceleration, and transport. SEPs also have practical implications as a potential radiation hazard, both for manned and unmanned space missions. Recent efforts have produced new quantitative SEP models that are steadily improving in their ability to confront these observations (Ng et al. 1999, 2003; Zank et al. 2000; Rice et al. 2003; Li et al. 2003; Li & Zank 2005; Lee 2005; Kocharov & Torsti 2003; Roussev et al. 2004; Sokolov et al. 2004).

One particular challenge for SEP modeling is the large event-to-event variability in elemental composition and spectral shapes at energies above a few tens of MeV per nucleon. Figure 1 illustrates this problem by comparing the energy dependence of the event-integrated Fe/O ratio in the events of 2002 April 21 and 2002 August 24. These two events have been put forward as particularly good exemplars of the high-energy variability because they arose from ostensibly similar CMEs and flares. From $\sim$0.5 to $\sim$10 MeV nucleon^{-1} the Fe/O ratios in the two events are nearly identical. But at higher energies, the events diverge, so that Fe/O eventually differs by nearly 2 orders of magnitude. In the 2002 April 21 event, the Fe/O ratio falls to only $\sim$10% of the nominal coronal value. In the 2002 August 24 event, on the other hand, Fe/O attains $\sim$6 times the coronal value, comparable to values found in small, ^{3}He-rich impulsive SEP events that originate from flares (Reames 1995). Both events erupted from near the west limb, and in neither case was there a significant particle increase above $\sim$1 MeV nucleon^{-1} when the weak flank of the associated shock arrived at Earth. These high-energy particles were therefore produced primarily near the Sun. The high-energy behavior is thus providing an important clue to the details of the acceleration processes that occurred there.

Tylka et al. (2005) have hypothesized that the variability in Figure 1 results from the interplay of two factors: evolution in the geometry of the CME-driven shock, which generally begins as quasi-perpendicular near the Sun but evolves toward quasi-parallel as the shock moves outward; and a compound seed population, typically comprising at least suprathermals from the corona or solar wind and suprathermals from flares. A simple analytical implementation of the shock-geometry hypothesis has demonstrated promise in accounting for the observed variability in the high-energy SEP data (Tylka & Lee 2006). However, there are also other scenarios in which accelerators other than a CME-driven shock dominate, or at least make significant contributions to, the SEP production at high energies (Cane et al. 2002; Kocharov et al. 2005; Klein & Posner 2005; Miroshnichenko et al. 2005), at least in some events.

In this paper, we present additional details on time structure, spectral shapes, and elemental composition for the events shown in Figure 1, based on the combined measurements from instruments on the *Advanced Composition Explorer* (*ACE*), *Wind*, and *GOES*. These results particularly emphasize the significant differences between the energetic particle characteristics of the two events. These data should be useful in testing hypotheses about the origins of SEP variability and in validating future numerical SEP models. We also briefly review characteristics of the associated activity, pre-event conditions, and onset timing.

[1] E. O. Hulburt Center for Space Research, Naval Research Laboratory, Code 7652, Washington, DC 20375; allan.tylka@nrl.navy.mil.
[2] California Institute of Technology, MC 220-47, Pasadena, CA 91125; cohen@srl.caltech.edu; rmewaldt@srl.caltech.edu.
[3] Consultant, 13 South Parkway, Prospect Heights, IL 60070; dietrich@odysseus.uchicago.edu.
[4] Space Science Center and Institute for the Study of Earth, Oceans, and Space, University of New Hampshire, Durham, NH 03824-3524; marty.lee@unh.edu.
[5] Bell Laboratories, Lucent Technologies, 600 Mountain Avenue, Murray Hill, NJ 07974; cgm@bell-labs.com.
[6] NASA Goddard Space Flight Center, Code 661, Greenbelt, MD 20771; reames@milkyway.gsfc.nasa.gov.
[7] Department of Astronomy, University of Maryland, College Park, MD 20742; cheeng@lheapop.gsfc.nasa.gov.

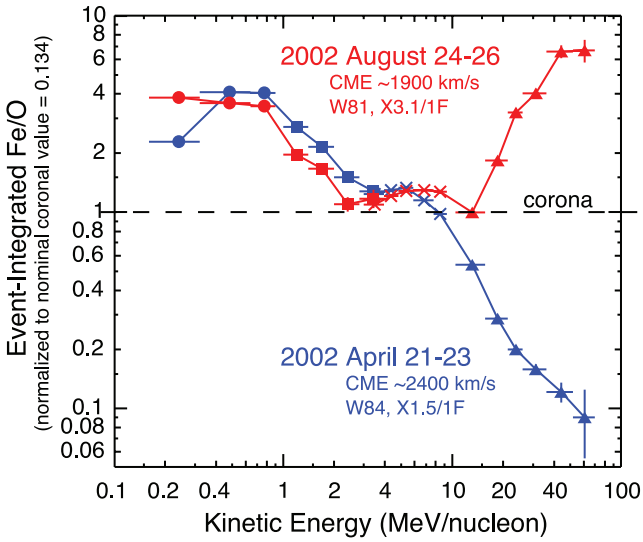

FIG. 1.— Event-integrated Fe/O (normalized to the nominal coronal value 0.134; Reames 1995) vs. energy for the solar energetic particle (SEP) events of 2002 April 21 (*blue*) and 2002 August 24 (*red*). In both events, the event integration was for 72 hr. Data come from the Ultra Low-Energy Isotope Spectrometer (ULEIS; Mason et al. 1998; *filled circles*) on *ACE*, the Electron Proton, and Alpha Monitor (EPAM; Gold et al. 1998; *filled squares*) on *ACE*, the Low Energy Matrix Telescope (LEMT) in the Energetic Particle Acceleration, Composition, and Transport (EPACT) experiment (von Rosenvinge et al. 1995; *crosses*) on *Wind*, and the Solar Isotope Spectrometer (SIS; Stone et al. 1998a; *filled triangles*) on *ACE*.

2. OVERVIEW OF EVENT CHARACTERISTICS

Table 1 summarizes characteristics of these two events. As already noted, both events were associated with very fast halo CMEs from source regions near the west limb of the Sun. The associated flares had nearly the same size. Both events were accompanied by metric and DH type III and type II radio emissions. Solar-wind speeds observed near Earth at the start of the events were also comparable. The interplanetary shocks associated with these two events had Sun-Earth transit times that were the same to within ~10%. (See Tylka et al. 2005 for further discussion.)

Perhaps the most striking *difference* in Table 1 is the number of flares generated by the active regions that spawned these two major particle events: the active region of the August event produced ~5 times as many optical and X-ray flares in the preceding 4 days as the April event. As discussed further in § 3, this difference in flare activity apparently had significant implications for the character of the suprathermal seed populations that were encountered by subsequent shocks.

These two events also show more subtle differences in the size and magnetic complexity of the active regions, the fitted CME acceleration, the durations and rise times of the flares, and the frequency range and duration of the DH type II radio emission. These quantities may provide useful diagnostics and constraints for modeling these events. However, their potential implications, if any, for the physics of particle acceleration near the Sun are not understood at present.[8]

3. PRE-EVENT CONDITIONS

One important objective for the next generation of SEP models is to take into account a realistic description of the preceding state of the corona and interplanetary medium. Kahler (2001) pointed out that the largest SEP events often occur in the wake of earlier events, which probably augmented the pool of accessible seed particles. Figure 2 suggests that there may have been striking differences between the seed populations in the SEP events we consider here. The figure shows hourly Fe and O intensities for five energy bins, from 40 keV nucleon^{-1} to 3.2 MeV nucleon^{-1}, over the 4 days preceding these two events. Time profiles prior to the 2002 April 21 event were complicated due to the 2002 April 17 halo CME. But note that the Fe and O timelines in the April event are almost always separated, so that Fe/O is more or less ~0.1, the nominal solar-wind/coronal value, at all energies. In the August event, on the other hand, the Fe and O timelines lie nearly on top of each other, so that Fe/O ~ 1 at all five energies. A large part of the pre-event population in the 2002 August 24 event may be associated with the very large impulsive event of 2002 August 20 (Leske et al. 2003; Reames & Ng 2004).

Of course, Figure 2 is merely suggestive. These pre-event populations are not literally the seeds for the SEP events: these observations were made at 1 AU, not at the base of the Sun-Earth field line. It is probably for this reason that attempts to correlate pre-event particle composition at 1 AU with that of the subsequent SEPs have generally been unsuccessful. But in these particular events, the pre-event Fe/O was constant for a long period of time and over a wide range of energies, perhaps making it more likely that they are indeed representative of at least part of the potential seed populations closer to the Sun.

However, the energy bins shown in Figure 2 cannot represent the entire seed population. In particular, the similarity of the two SEP events below ~10 MeV nucleon^{-1} (Fig. 1) implies that those ions were accelerated out of seeds where there were smaller compositional differences between the events. Presumably, those seeds were at even lower energies than those shown here.

Pre-event conditions other than seed populations may also be relevant to the differences between these two events. Gopalswamy et al. (2004) demonstrated that the presence or absence of a preceding CME (erupting from the same active region, less than 24 hr earlier) helps to account for differences between high- and low-intensity SEP events. They suggested that these differences could be the consequences of several factors, including modification of the primary shock due to changes in the magnetic field and density of the medium into which it propagates. In the cases of the two events we are considering here, both were preceded by another CME. According to Gopalswamy et al. (2004), the CME of 2002 April 21 followed so closely on the heels of a preceding CME that it would have overtaken it within the occulting disk of the LASCO coronagraph. For the 2002 August 24 event, they estimated that the initial separation of the CMEs was 21.5 Rs. Richardson & Cane (1996), Bieber et al. (2002), and Ruffolo et al. (2006) showed that preceding CMEs can alter the topology of the interplanetary magnetic field in ways that significantly affect particle transport from the Sun. According to the list of interplanetary CMEs provided by Cane & Richardson (2003), Earth was located within an interplanetary CME at the start of the April event, but not during the August event.

4. ONSET TIMING

A rich phenomenology accompanies the start of a major solar particle event. These other observations, and their sequence of occurrence, provide important context for understanding the drivers behind the particle acceleration. Figure 3 compares the observed onset times at Earth to the time profiles of 1 minute–averaged proton intensities at ~165–500 MeV from *GOES-8*. Table 2 lists the onset times. In the table, the onset times of the

[8] These two events are SHINE campaign events. A compendium of side-by-side comparisons of solar and interplanetary observations, as well as additional information on particle spectra and composition, is available at http://cdaw.gsfc.nasa.gov/CME_list/SHINE2003/index.html.

TABLE 1
SOLAR AND INTERPLANETARY CHARACTERISTICS

Parameter	2002 April 21	2002 August 24
Active Region Characteristics[a]		
NOAA number	9906	10069
Sunspot area (10^{-6} solar hemispheres)	~810	~1535
Magnetic classification	Bg	Bgd
Number of optical flares, preceding 4 days	13	62
Number of X-ray flares, preceding 4 days	5	35
CME Characteristics[b]		
Width	Halo	Halo
Linear-fit speed[b] (km s^{-1})	2393	1913
Quadratic-fit speed[b] (km s^{-1})	2391	1992
Acceleration (m s^{-2})	−1.4	43.7
Flare Characteristics[c]		
Size	X1.5/1F	X3.1/1F
Solar location	S14°, W84°	S02°, W81°
Soft X-ray time-to-maximum (minutes)	68	23
Hα time-to-maximum (minutes)	32	8
Soft X-ray duration (minutes)	115	42
Hα duration (minutes)	112	28
Radio Characteristics[c,d]		
Culgoora metric type III:		
Frequency range (MHz)	<57–470	<57–1600
Duration (minutes)	7	6
Maximum intensity class	1	3
Culgoora metric type II:		
Frequency range (MHz)	<57–130	<57–190 (SH)
Duration (minutes)	11	8
Intensity class	3	2
Wind WAVES DH type II:		
Frequency range (kHz)	60–10000	400–5000
Duration (hr)	22.5	1.7
Solar-Wind Speed		
Solar-wind speed[e] (km s^{-1})	484 ± 10	393 ± 16
Associated Shock at Earth[f]		
Transit time from Sun (hr)	52	58
Velocity jump (km s^{-1})	~190	~50

[a] As reported at http://sec.noaa.gov/weekly/index.html.
[b] As given in the *SOHO* LASCO (Brueckner et al. 1995) catalog at http://cdaw.gsfc.nasa.gov/CME_list/, as of 2005 October 27. Due to revisions in the catalog, the values here are slightly different from earlier reports. Speeds are as determined by linear and quadratic fits to the CME height-time profiles. The quadratic-fit speed is evaluated at 20 Rs.
[c] From SGD Online at http://sgd.ngdc.noaa.gov/sgd/jsp/solarindex.jsp.
[d] For uniformity of comparison, only Culgoora metric results are shown here; Hiraiso and other station reported similar values. Metric type III characteristics span multiple small groups of bursts. The cited intensity class is that of the most intense burst. *Wind* WAVES (Bougeret et al. 1995) results are from http://lep694.gsfc.nasa.gov/waves/waves.html. Type III bursts are also evident in the *Wind* WAVES frequency range.
[e] Average and standard deviations from ~1 minute–averaged values during ±3 hr of the event onset, from the Solar Wind Experiment (SWE; Ogilvie et al. 1995) on *Wind* as given at http://cdaweb.gsfc.nasa.gov/cdaweb/sp_phys/.
[f] Estimated from *Wind* SWE data.

various photon emissions have been corrected back to the Sun, by subtracting 8.3 minutes from the time of observation at Earth.

Also listed in Table 2 are particle onset times for the highest-energy proton and electron observations available to us in these two events. The values in parentheses are the observed time of first arrival at Earth, as determined by >2 σ increases over preceding background levels. The August event was a ground-level event (GLE). The earliest observed particle onset in the August event comes from 5 minute averages in the Apatity neutron monitor, which showed a 2.4 σ increase at 01:14–01:19 UT. The anticoincidence shield surrounding the University of Chicago's Cosmic-Ray Nuclei Experiment (CRNE; Garcia-Munoz et al. 1975) on *IMP-8* registered a 3.1 σ increase at 01:20 UT. (This anticoincidence shield is sensitive to relativistic protons with energies of a

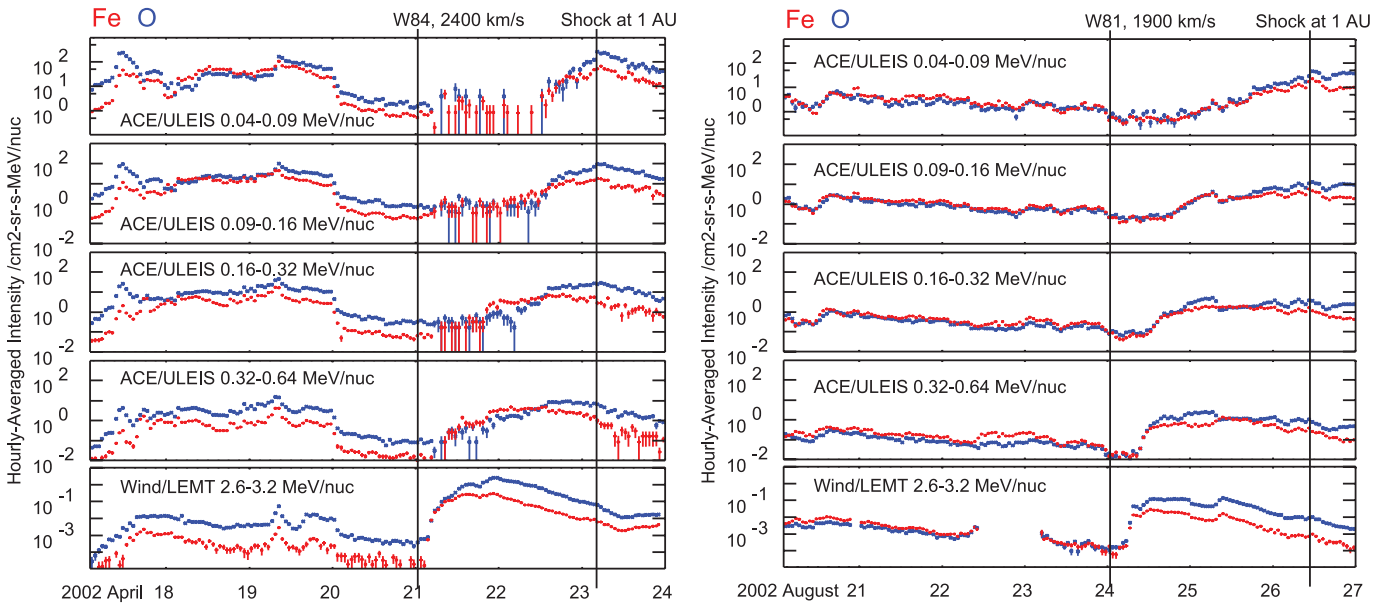

FIG. 2.—Fe (*red*) and O (*blue*) timelines at five energies, from 40 keV nucleon^{-1} to 3.2 MeV nucleon^{-1}, including the 4 days preceding the 2001 April 21 (*left*) and 2002 August 24 (*right*) events. Vertical lines mark the launch of the CME and the arrival of the associated shock at 1 AU. Time profiles prior to the April event were complicated due to the 2002 April 17 halo CME. The pre-event population in the August event may be associated with the 2002 August 20 event (Leske et al. 2003). *ACE* ULEIS was affected by reduced collecting power during the onset of the April event, and *Wind* LEMT had a data gap on 2002 August 22–23.

few GeV, while the surrounding satellite material effectively absorbs electrons.) A high-energy proton channel on *GOES-8* showed a 2.4 σ increase at 01:24 UT. *IMP-8* CRNE also registered a 2.6 σ increase in >2 MeV electrons at 01:23 UT; *ACE* EPAM data show a 2.4 σ increase in their highest-energy electron channel at 01:24 UT.

We have less information on high-energy particle onsets in the April event: this event was not a GLE and *IMP-8* telemetry was not recovered. Onset determinations in this event are also less precise because of its comparatively slow rate of rise (see Fig. 3). Our best estimate for the proton onset in the April event comes from *GOES-8*, which showed >2 σ excesses (but with some downward fluctuations) in minute-averaged data starting at 01:41–01:47 UT. *ACE* EPAM recorded a 2.4 σ increase in its highest-energy electron channel at 01:36 UT.

Table 2 also gives the times of particle release from the Sun. These times were derived by assuming nominal Parker-spiral path lengths (1.12 and 1.17 AU for the April and August events, respectively, based on the solar-wind speeds in Table 1), scatter-free transport for the first-detected particles, and estimated speeds for the first-detected particles, as also noted in Table 2. The proton-release times derived in this way from *GOES-8*, *IMP-8*, and Apatity in the August event are consistent to within uncertainties. To within uncertainties, the electron and proton release times are the same in the August event. The inferred proton release time in the April event is $\sim$8$\pm$3 minutes later than the electron release time, but this delay may be an artifact of limited instrumental sensitivity and the comparatively slow rate of rise in this event.

By comparing with *SOHO* LASCO observations (Yashiro et al. 2004), we estimate the heights of the CMEs' leading edges at the times of particle release as 5.5 $\pm$ 0.6 and 3.8 $\pm$ 0.5 Rs from Sun center in the April and August events, respectively. However, high particle backgrounds, limited instrumental sensitivity, possible scattering of the first-detected particles, deviations of the field line from the nominal Parker-spiral configuration, and uncertainties about the energies of the first-detected particles all tend to imply that the particles' actual times of departure from the Sun might have been earlier than our estimates. Our CME-height estimates are therefore probably best interpreted as upper limits that constrain modeling efforts.[9]

Finally, note the difference in the rise times of the particle profiles in Figure 3. For the August event, the fitted *e*-folding time of the rise in the first 10 minutes is 149 $\pm$ 14 s. The same procedure applied to the higher resolution *IMP-8* CRNE data yielded an *e*-folding time of 132 $\pm$ 2 s. For the April event, on the other hand, the fitted *e*-folding time is $\sim$5 times longer at 768 $\pm$ 114 s. Source longitude is well known to affect rise times (Cane et al. 1988; Reames et al. 1996), but that is not relevant in these two events. A higher level of interplanetary scattering can also stretch out the rise to maximum; that may be a factor in Figure 3, although it is perhaps worth noting that both of these events appear on the *ACE* EPAM list of beamed electron events.[10] At sufficiently high energies, the rise times can also reflect the acceleration timescale at the source. If that be the case here, the apparent difference in Figure 3 is qualitatively consistent with the shock-geometry hypothesis, since the acceleration rate can be much faster in quasi-perpendicular shocks (Jokipii 1987; Webb et al. 1995). However, such an inference requires detailed studies of additional events. In any case, the difference in rise times in Figure 3 should also be addressed while modeling other aspects of these two events. We

[9] Solar particle release times and the corresponding CME-heights are better determined in other events. More reliable results can be derived from velocity dispersion among the onset times at different energies (e.g., Tylka et al. 2003; see also Sáiz et al. 2005 and Lintunen & Vainio 2004). However, applying this method to these two events has proven difficult because of the high pre-event backgrounds and the relatively slow rate-of-rise in the April event. In addition, at the onset of the August event, the interplanetary magnetic field vector lay outside the *ACE* SIS field of view, so that the first arrival of high-energy ions was not recorded. Onsets in ground-level events have also been precisely determined by using a sophisticated transport model to fit both intensity profiles and anisotropies from the Spaceship Earth neutron monitor network (e.g., Bieber et al. 2002, 2004). The relatively small size of the August GLE poses a challenge for this method. Nevertheless, a preliminary analysis of the Spaceship Earth response to the August event derived a solar release time of 01:08 UT $\pm$2 minutes (presentation at the 2004 SHINE meeting, J. W. Bieber et al.). This time is consistent with our result.

[10] See http://www.srl.caltech.edu/ACE/ASC/DATA/level3/.

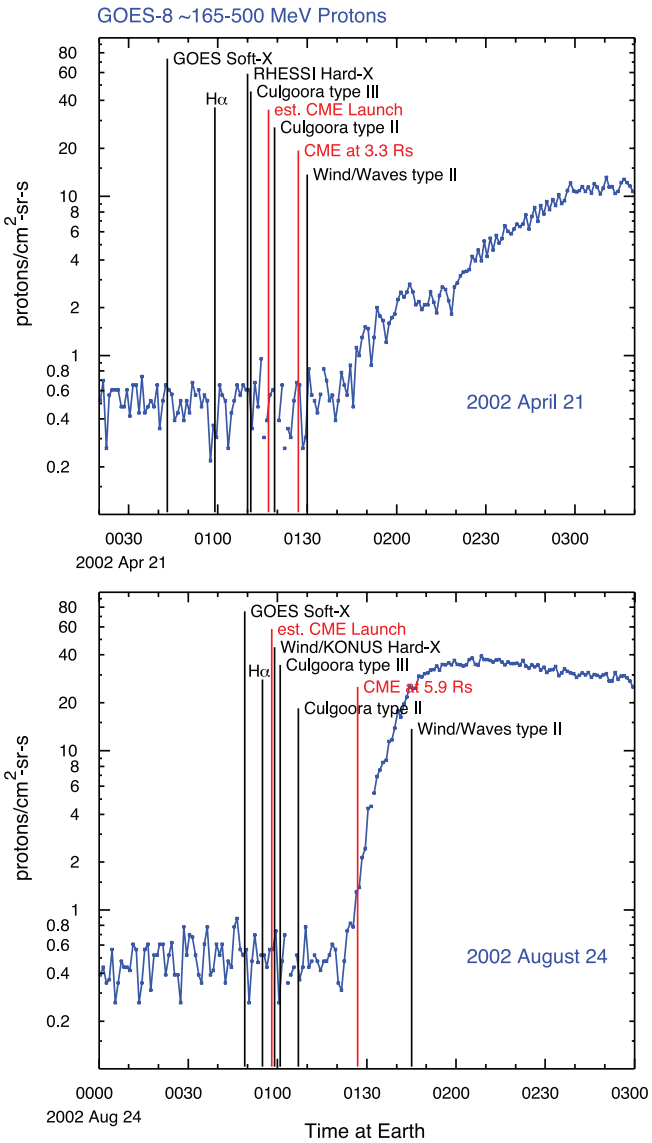

FIG. 3.—Intensities of 1 minute–averaged protons at ~165–500 MeV from *GOES-8* over 3 hours spanning the start of the events on 2002 April 21 (*top*) and on 2002 August 24 (*bottom*). These are the highest-energy data for which we have high-time resolution at the onsets in both events. For comparison, black vertical lines mark the onsets of various radio and photon emissions at Earth. Red vertical lines show the time of the first LASCO CME image, as well as the estimated CME launch, as inferred from linear fits to the CME height-time profiles.

now return to energetic ion characteristics, which are the main focus of this paper.

5. TIME-DEPENDENT Fe/O

Figure 1 pointed out differences in the event-integrated Fe/O. But additional information is contained in the time-dependent composition. Figures 4 and 5 compare Fe/O versus time at various energies for the two events. These data are complicated and require detailed modeling. But as we suggest below, the time dependence of Fe/O provides some qualitative indications on the relative Q/A values of O and Fe and hence the seed populations. Specifically, the time dependence of Fe/O in the April event suggests that iron has significantly lower Q/A than oxygen at all energies, as would be expected from a seed population dominated by coronal or solar-wind suprathermals. This is also true below ~15 MeV nucleon^{-1} in the August event. But the Fe/O time profiles suggest that the Q/A difference between the two ions becomes smaller as energy increases in the August event. This behavior would be consistent, at least qualitatively, with a compound source population, in which flare particles preferentially provide the seeds for higher energy ions.

Figure 4 compares the two events in three energy bins at 2.5–10 MeV nucleon^{-1} from the Low-Energy Matrix Telescope (LEMT; von Rosenvinge et al. 1995) on *Wind*. The bottom panels show the oxygen intensities, which are larger in the April event but exhibit more complicated structure in the August event. Overall, however, the events are rather similar. The most striking feature in Figure 4 is the decline in Fe/O from initially enhanced values during the rise phase of the event. This behavior is qualitatively consistent with particle transport in which Fe scatters less than O (Parker 1963; see also Ng et al. 2003, Appendix C). Since the scattering mean free path generally increases with rigidity, this initial drop in Fe/O suggests than Fe has a significantly smaller Q/A than O. The drop-off of Fe/O at the highest energy bin is also more pronounced in the April event, a reflection of the greater steepening in the iron spectrum relative to that of oxygen in this event.

Figure 5 shows the same quantities in four energy bins at 10–40 MeV nucleon^{-1} from the Solar Isotope Spectrometer (SIS; Stone et al. 1998a) on *ACE*. At the lowest energy bin (10–15 MeV nucleon^{-1}), the oxygen profiles are very similar (except for normalization). The Fe/O profiles at this energy are also nearly identical for the two events, dropping by more than an order of magnitude in the first 12 hr. But at higher energies, the behavior of Fe/O diverges in the two events. In the April event, a similar drop is also seen at the energies above 15 MeV nucleon^{-1}, and at all times Fe/O decreases with increasing energy. This behavior is qualitatively consistent with Fe at these energies also having a relatively low Q/A in the April event. In the August event, on the other hand, Fe/O increases with energy at all times, except possibly the first 3 hours. Moreover, as energy increases, the drop in Fe/O becomes less pronounced: whereas Fe/O at 10–15 MeV nucleon^{-1} drops by a factor of ~20 as time goes on, Fe/O at 30–40 MeV nucleon^{-1} decreases by only a factor of 3. Transport therefore apparently makes less distinction between Fe and O at high energies in the August event, suggesting that Q/A of Fe and O at high energies are more similar than they are at lower energies.

Finally, Figure 6 looks at the time dependence in Fe/O in a different way, by plotting Fe/O versus energy at various times during the first 9 hr of the two events. The roughly exponential drop of Fe/O with energy is clear at all times in the April event. In the August event, there is no strong energy dependence in Fe/O in the first ~3 hr. But after that, Fe/O above ~10 MeV nucleon^{-1} increases roughly as a power law with energy.

6. EVENT-AVERAGED SPECTRA, INFERRED IONIC CHARGE STATES, AND ELEMENTAL COMPOSITION IN THE 2002 APRIL 21 EVENT

Figure 7 shows event-averaged spectra for the major elements[11] in the 2002 April 21 event. Also shown for each element is a least-squares fit to the familiar Ellison & Ramaty (1985) form,

$$F_X(E) = C_X E^{-\gamma_X} \exp(-E/E_{0X}),$$

[11] We were unable to make a comprehensive fit to the He spectrum due to large instrument-to-instrument discrepancies in the intensities. The instruments also reported significantly different He/C ratios, perhaps indicating some instrumental problems in the He measurements. We nevertheless estimated power-law indices for He at low energies (Fig. 8) by averaging the fitted values from individual instruments. In Figs. 11 and 12, we also include an estimate of the He/C ratio, derived by averaging among the instruments. Because of the instrument-to-instrument discrepancies, these He results are reported with large error bars.

TABLE 2
ONSET TIMES AT THE SUN

Observation	UT 2002 April 21	UT 2002 August 24
GOES soft X-rays[a,b]	00:35	00:41
Hα[a,b]	00:51	00:47
Hard X-rays[a,c] (>50 keV)	01:02	00:51
Metric type III[a,d]	01:03	00:53
Estimated CME launch[a,e]	01:09	00:50
Metric type II[a,d]	01:11	00:59
DH type II[a,f]	01:22	01:37
Particle Release Times[g]:		
Neutron monitor protons ($v = 0.95c$)	n/a	01:07 (01:17 $\pm$ 3 minutes)[h]
IMP-8 CRNE relativistic protons ($v = 0.95c$)	n/a	01:10 (01:20)
GOES-8 165–500 MeV protons[i] ($v = 0.76c$)	01:31 (01:44 $\pm$ 3 minutes)	01:11 (01:24)
IMP-8 CRNE >2 MeV electrons ($v = 0.98c$)	n/a	01:13 (01:23)
ACE EPAM 175–312 keV electrons[j] ($v = 0.73c$)	01:23 (01:36)	01:11 (01:24)

[a] Light-travel time of 8.3 minutes has been subtracted from the observed onset time at Earth.
[b] From SGD Online at http://sgd.ngdc.noaa.gov/sgd/jsp/solarindex.jsp.
[c] From *RHESSI* (Lin et al. 2002) for the April event and from the *Wind* Konus experiment (Aptekar et al. 1995; data at http://lheawww.gsfc.nasa.gov/docs/gamcosray/legr/konus/) for the August event (*RHESSI* was occulted at the onset of the August event).
[d] Culgoora results, as reported at http://sgd.ngdc.noaa.gov/sgd/jsp/solarindex.jsp.
[e] As given in the *SOHO* LASCO (Brueckner et al. 1995) catalog at http://cdaw.gsfc.nasa.gov/CME_list/, as of 2005 October 27. These values are from linear fits to the height-time profiles. For the August event, a quadratic fit to the height-time profile yielded an estimated launch time that is 5 minutes earlier.
[f] *Wind* WAVES (Bougeret et al. 1995), as reported at http://lep694.gsfc.nasa.gov/waves/waves.html.
[g] Particle release times from the Sun, after correction for travel time to Earth, as described in the text and using the noted values v for the assumed speeds of the first-detected particles. The times of first detection at Earth (given in parentheses) were identified as a >2 σ increase over preceding background levels. Uncertainties are $\pm$1 minute, unless stated otherwise.
[h] Based on a 2.4 σ increase over preceding background at 01:14–01:19 at the Apatity neutron monitor, http://pgi.kolasc.net.ru/CosmicRay/.
[i] From 1 minute–averaged rates available from http://spidr.ngdc.noaa.gov.
[j] From $\sim$10 s–averaged data, available at http://data/ftecs/com/archive/ace_epam/index.html. The times reported here have been corrected for the EPAM data processing error that was announced on 2006 April 13 (see http://sd-www.jhuapl.edu/ACE/EPAM).

where E and E_{0X} are in units of MeV nucleon^{-1} and each species X was fitted independently to derive values for the parameters C_X, γ_X, and E_{0X}. Except for H and Fe, the fits have reduced χ^2 values of order unity for $\sim$20 degrees of freedom, as noted in each panel. To attain these χ^2 values, we added 15% systematic uncertainty in quadrature with the (generally negligible) statistical error on each measurement.[12] Root mean square (rms) deviations of the residuals from the fitted function (which are typically $\sim$15%–20%, except for H and Fe) are also noted in each panel. Additional technical details about the systematic uncertainties, data selection, and fitting procedure are given in the Appendix.

In the case of H, the poor χ^2 may indicate that the systematic uncertainties in the proton measurements are even larger than we have assumed. For Fe, the large χ^2 is driven by measurements below $\sim$1 MeV nucleon^{-1}, where the observed spectrum is clearly more complicated than a simple power law. Nevertheless, it is remarkable that such a simple functional form describes these spectra so well.

Figure 8 shows the fitted power-law indices γ_X and e-folding energies E_{0X} plotted versus atomic number. All of the power-law indices agree to within $\sim\pm$5%. Except for Fe, the fitted power-law indices are also within 2 standard deviations of a common mean.

[12] This systematic uncertainty generally compensates for instrument-to-instrument discrepancies. However, we do not intend to suggest that instrumental systematic errors are necessarily this large. Rather, this systematic uncertainty also reflects the precision to which a simple functional form can represent what is actually a time integral over a complex phenomenon. The timelines in Figs. 2, 4, and 5 all show detailed structure, which cannot be accounted for in a simple way. It should also be remembered that the various instruments average over different lookout directions, so that discrepancies also can arise whenever the particle distributions are not isotropic.

Although the power-law indices are nearly identical for all species, the e-folding energies clearly differ, as shown in the middle panel of Figure 8. Fe has a substantially smaller e-folding energy than the lighter ions, and this fact leads to the suppressed Fe/O at high energies (Fig. 1).

As shown in Figure 9, *Wind* LEMT has spectral information on trans-Fe ions (Reames 2000; Reames & Ng 2004) with atomic numbers $34 \leq Z \leq 40$ in this event. The data are too sparse to support a full spectral fit. We therefore performed a constrained fit, in which the power-law index was held at the mean value determined from the other species, but the normalization coefficient and e-folding energy were free parameters. The e-folding energy for the trans-Fe ions is also plotted in Figure 8. It is even smaller than that of Fe.

As suggested by Ellison & Ramaty (1985) and as demonstrated by Tylka et al. (2000), these e-folding energies scale linearly with the ions' Q/A values, at least in some events. We can therefore try to exploit this dependence, in order to derive mean charge states for the individual species. To do this, we begin with oxygen, which has the best-measured spectrum. The *Solar, Anomalous, and Magnetospheric Particle Explorer* (*SAMPEX*; Cook et al. 1995) has reported a mean ionic charge state of $\langle Q_O \rangle = 6.3 \pm 0.4$ for oxygen at $\sim$17–70 MeV nucleon^{-1} in this event (Labrador et al. 2003; A. Labrador 2003, private communication). We infer the mean ionic charge state of the other species by scaling linearly from this value according to the fitted e-folding energies; that is,

$$Q_X = Q_O(A_X/16)(E_{0X}/E_{0O}),$$

where $E_{0O} = 11.34 \pm 0.34$ MeV nucleon^{-1} is the fitted e-folding energy from the oxygen spectrum.

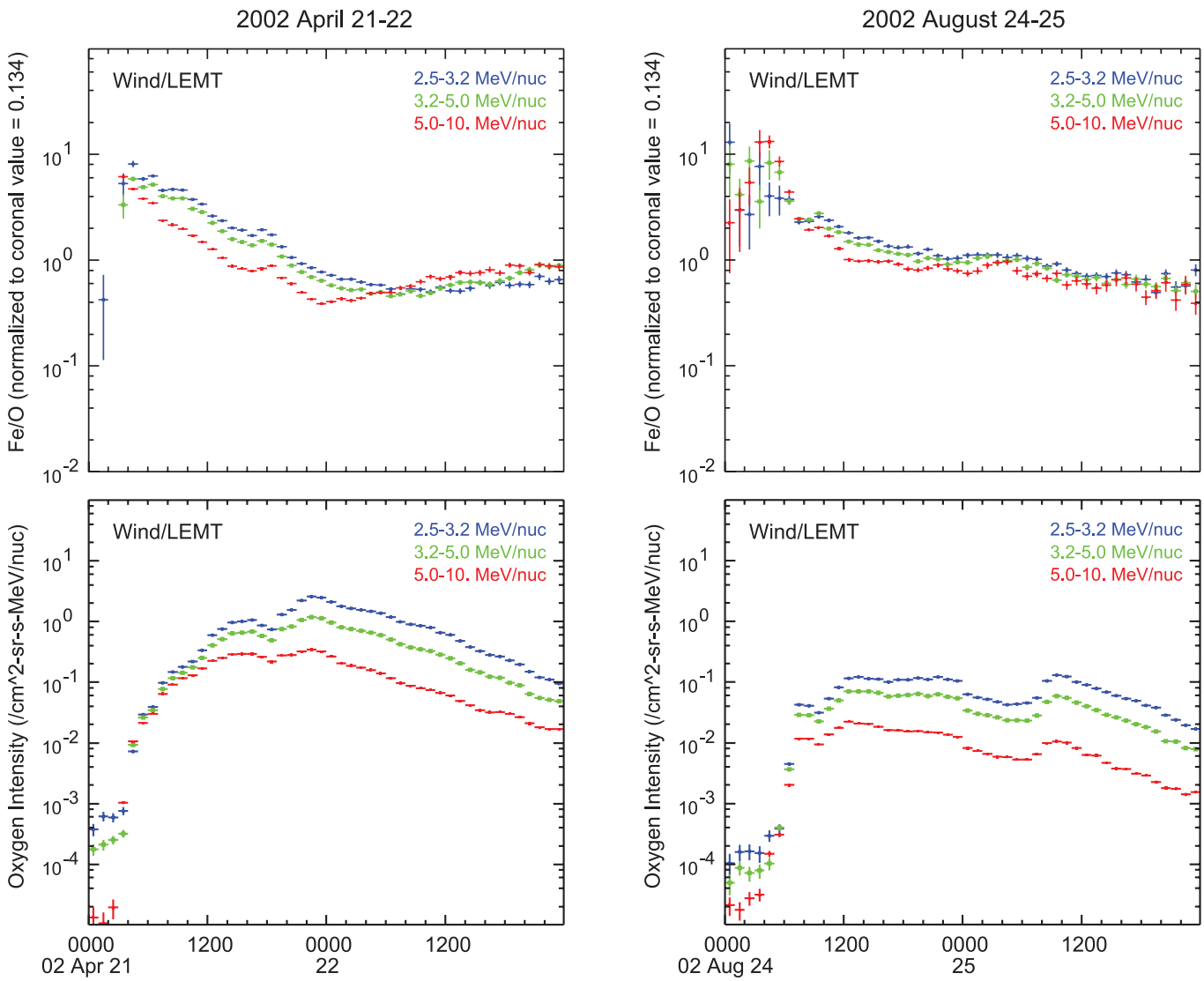

FIG. 4.—Fe/O (normalized to the nominal coronal value 0.134; *top panels*) and oxygen intensity (*bottom panels*) vs. time in the 2002 April 21 (*left*) and 2002 August 24 (*right*) events from *Wind* LEMT in three energy bins covering 2.5–10 MeV nucleon^{-1}, as distinguished by colors. The data points are 1 hr averages.

The inferred charge states are plotted versus atomic number Z in the bottom panel of Figure 8. The inferred charge states are reasonable and thus confirm the assumed linearity to within $\sim$10%. For example, the inferred charge of protons is 1.2 ± 0.1, which is certainly acceptable given the imprecision in determining the proton e-folding energy from the wide high-energy bins from *GOES*. The inferred charge state of Ne ($\langle Q \rangle = 8.0 \pm 0.7$) is also as expected, since Ne should have $\langle Q \rangle \sim 8$ for a broad range of source-plasma temperatures. Finally, the charge states of Fe and the trans-Fe ions are nearly the same, which is also what one would generally expect (Post et al. 1977).

From these measured ionic charge states, one can use theoretical calculations to further infer the temperature of the source plasma (Arnaud & Rothenflug 1985; Arnaud & Raymond 1992; see also Reames et al. 1994, Fig. 14). These inferred temperatures are displayed for the various elements in Figure 10. The inferred temperatures for all species are consistent with a common temperature of 1.44 ± 0.10 MK. This temperature is well within the 1–2 MK range generally associated with the corona and solar wind.

Finally, we consider the relative elemental composition in this event. To do this, we calculate the ratio of the fitted normalization coefficient C_X for each species X to that of carbon, and then normalize the result to nominal coronal ratios (Reames 1995, 2000). By using the normalization coefficients C_X, we are focusing on energies below the e-folding energies, where spectral differences among the elements are small. Following Brenneman & Stone (1985), it is customary to examine relative abundances as a power law in Q/A. We used our inferred mean charges from Figure 8 to evaluate Q/A for ions heavier than He. Figure 11 shows the resulting correlation. The relative abundances are strongly anticorrelated with Q/A, as indicated by the correlation coefficient (-0.88). However, the reduced χ^2 (=10.1) of the resulting power-law fit is poor.

In Figure 12, we show an alternative correlation, in which the logarithm of the relative abundance is plotted versus the ion's mass number. In this case, the correlation coefficient (0.987) is only somewhat better than in Figure 11, but the fit quality (with reduced $\chi^2 = 1.2$) is substantially improved.[13] However, it is

[13] Of course, an equally good fit is obtained by plotting vs. atomic number Z. However, a *power law* in mass number A gives a lower correlation coefficient (0.801) and a substantially worse fit, with reduced $\chi^2 = 16.1$.

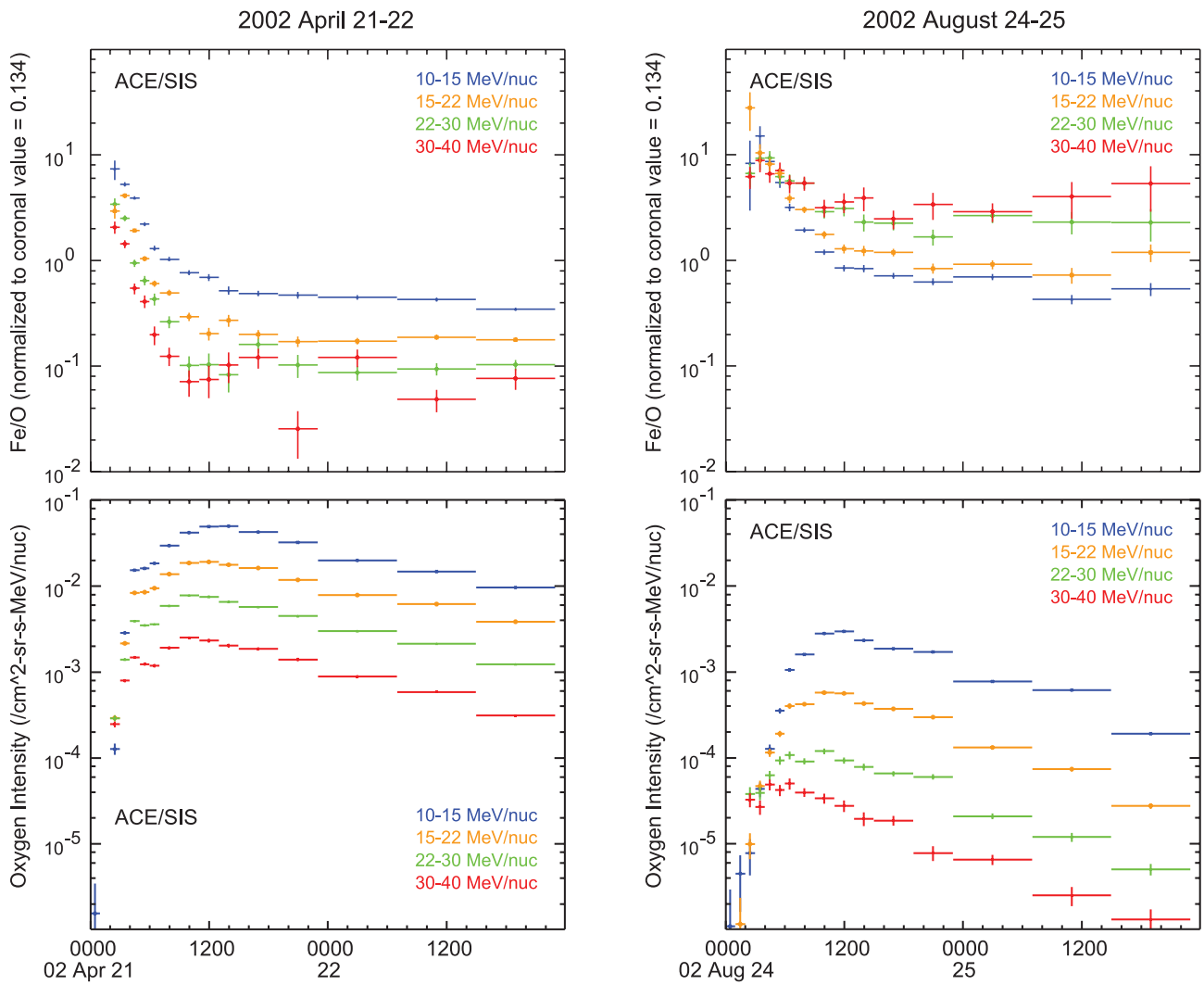

FIG. 5.—Fe/O (normalized to the nominal coronal value 0.134; *top panels*) and oxygen intensity (*bottom panels*) vs. time in the 2002 April 21 (*left*) and 2002 August 24 (*right*) events from *ACE* SIS in four energy bins covering 10–40 MeV nucleon^{-1}, as distinguished by colors. Hourly averages are shown in the first 5 hours of the event, but longer integration intervals are used later, when quantities are changing more slowly and/or ion statistics are smaller.

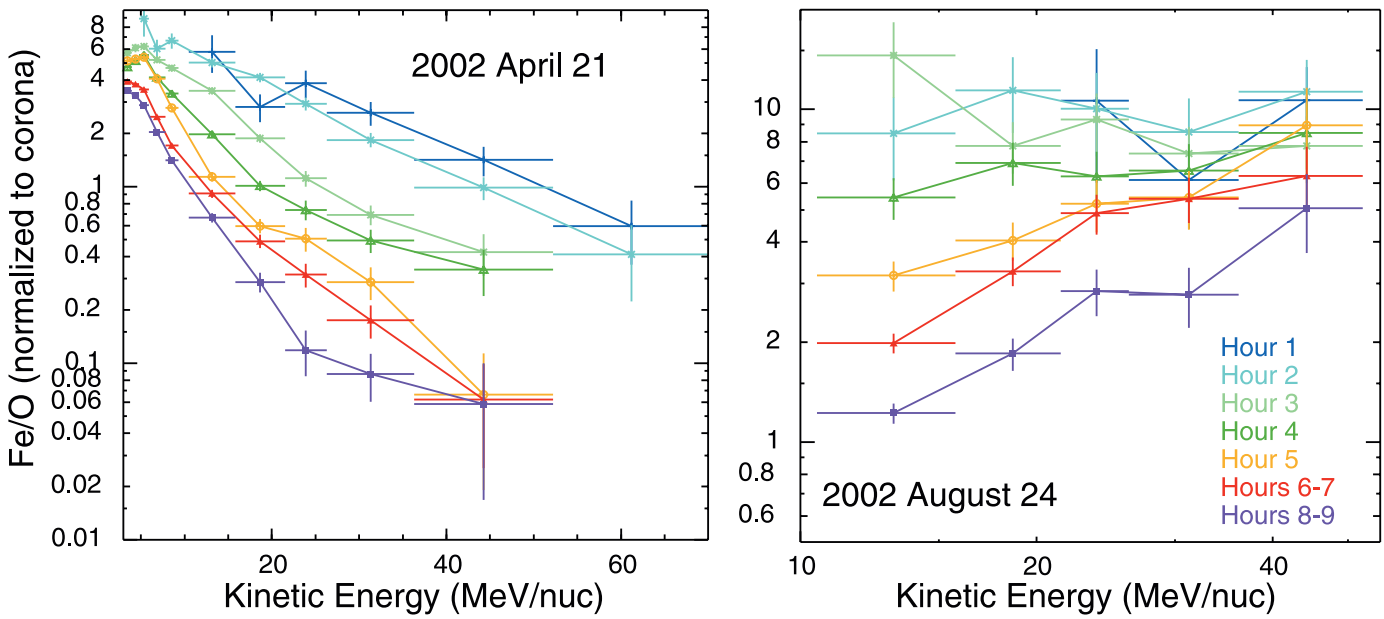

FIG. 6.—Fe/O (normalized to the nominal coronal value 0.134) vs. energy during the first 9 hours of the 2002 April 21 (*left*) and 2002 August 24 (*right*) events. Time intervals are distinguished by color, as shown in the legend at the right. Data points below 10 MeV nucleon^{-1} are from *Wind* LEMT; data points above 10 MeV nucleon^{-1} are from *ACE* SIS. Note the difference in the vertical scale on the two panels. The left panel is log-linear, so as to emphasize the nearly exponential drop in Fe/O with energy in the April event. The right panel is log-log, showing that after the first 3 hours of the August event, Fe/O above 10 MeV nucleon^{-1} increases with energy roughly as a power law.

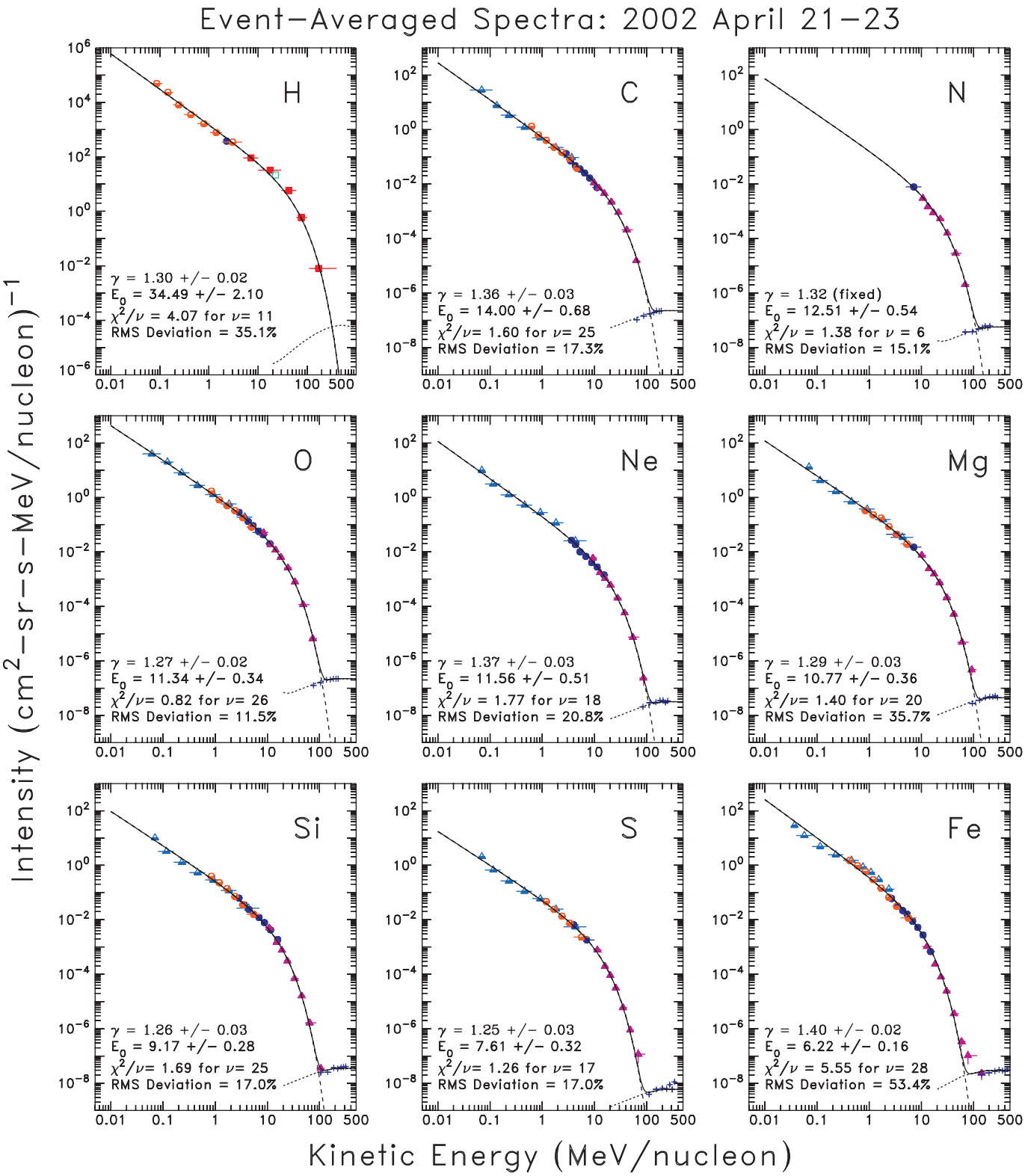

FIG. 7.—Event-averaged spectra for major elements in the 2002 April 21 solar particle event. The averaging interval began at 0:00 UT on 2002 April 21 and ended at 0:00 UT on 2002 April 24. Data are from *ACE* ULEIS (*light blue, half-filled triangles*), *ACE* EPAM (*orange, half-filled circles*), *Wind* LEMT (*dark blue, filled circles*), *ACE* SIS (*purple, filled triangles*), and *GOES-8* (protons >5 MeV; *red, filled squares*). Blue crosses in the lower right corners are Galactic cosmic ray (GCR) measurements from the Cosmic-Ray Isotope Spectrometer (CRIS; Stone et al. 1998b) on *ACE*. SEP intensities are fitted to the Ellison & Ramaty (1985) function (see text). Fit parameters, reduced χ^2, and rms deviation of the residuals are noted in each panel. For nitrogen, the power-law index has been fixed to the average value from the other species. In the lower right corners, short dashes show estimated GCRs, and long dashes are the extrapolated SEP fits. Solid curves show the sum of fitted SEPs and GCRs.

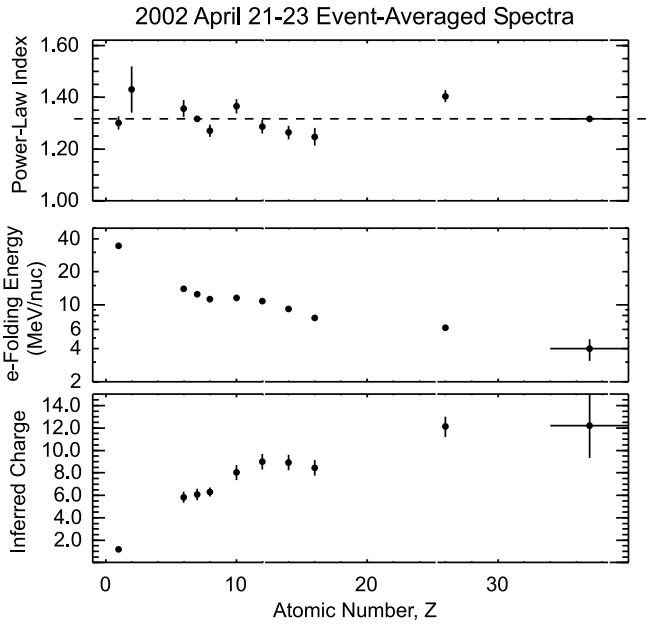

FIG. 8.—Fitted power-law indices (*top*), fitted *e*-folding energy (*middle*), and inferred mean ionic charge (*bottom*) plotted vs. atomic number Z for event-averaged energy spectra in the 2002 April 21 event. The dashed line marks the weighted average of the data points in the top panel. For the fits to nitrogen and to ions at $34 \leq Z \leq 40$, the power-law index (*top panel*) has been fixed to the average value from the other species. In the bottom panel, the oxygen charge state measurement (from which the others are derived, as described in the text) came from *SAMPEX* (Labrador et al. 2003).

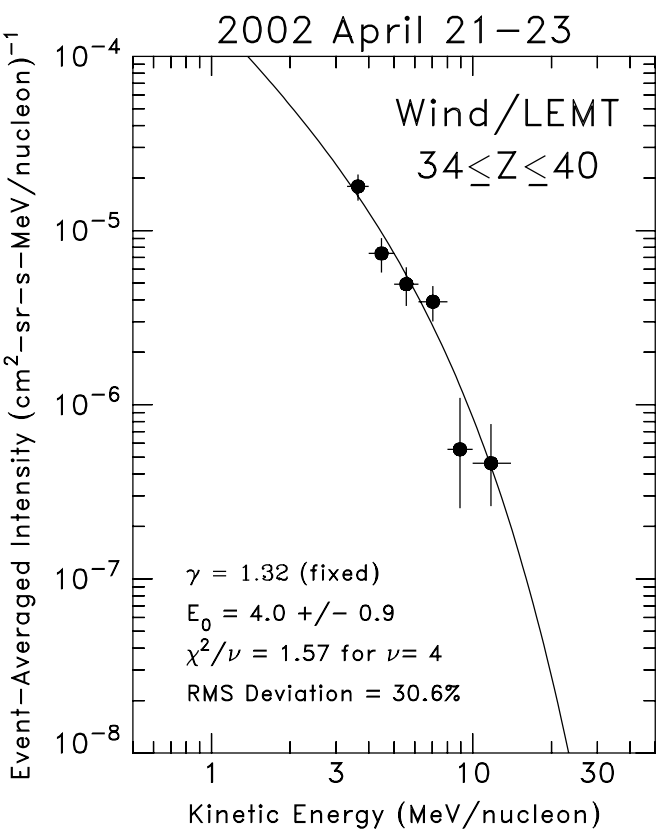

FIG. 9.—Event-averaged spectrum of ions with atomic number $34 \leq Z \leq 40$ from *Wind* LEMT in the 2002 April 21 event and its fitted Ellison & Ramaty spectrum, as described in the text. Data points are plotted with 1 σ Poisson error bars (Gehrels 1986).

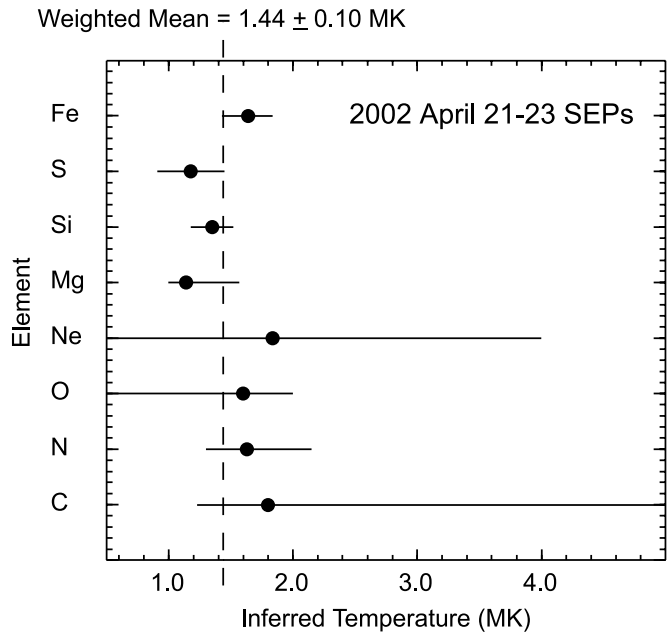

FIG. 10.—Source plasma temperatures (Arnaud & Rothenflug 1985; Arnaud & Raymond 1992), as inferred from the mean ionic charge states derived from spectral rollovers in the 2002 April 21 event.

not clear whether this exponential in A is inherent in the source population for this particular event, or whether it reflects another aspect of biasing during acceleration and transport processes.[14]

7. EVENT-AVERAGED SPECTRA AND ELEMENTAL COMPOSITION IN THE 2002 AUGUST 24 EVENT

Figure 13 shows event-averaged spectra for the 2002 August 24 event. Two differences between these spectra and those in the April event (Fig. 7) are immediately apparent. First, the exponential rollovers that govern high energies in the April event are absent here. Instead, each species shows one power law that smoothly evolves into a second, steeper power law, which describes the SEP spectra out to the highest measurable energies. Second, whereas Fe has the steepest spectrum in the April event (because of its comparatively low *e*-folding energy), Fe has the hardest spectrum among the heavy ions in the August event.

None of the species in Figure 13 shows spectral hardening, which would generally appear if there really were two independent accelerators operating at low and high energies, respectively, in this event. To quantitatively characterize the spectra, we therefore also show in Figure 13 fits to the Band et al. (1993) function. This function is a purely empirical form, first introduced in the context of gamma-ray burst studies. The Band et al. function for species X may be written as

$$F_{\rm X}(E) = C_{\rm X} E^{-\gamma_{a\rm X}} \exp(-E/E_{0\rm X}), \text{ for } E \leq (\gamma_{b\rm X} - \gamma_{a\rm X}) E_{0\rm X},$$

$$F_{\rm X}(E) = C_{\rm X} E^{-\gamma_{b\rm X}} [(\gamma_{b\rm X} - \gamma_{a\rm X}) E_{0\rm X}]^{(\gamma_{b\rm X} - \gamma_{a\rm X})} \times \exp(\gamma_{a\rm X} - \gamma_{b\rm X}), \text{ for } E \geq (\gamma_{b\rm X} - \gamma_{a\rm X}) E_{0\rm X},$$

[14] Dietrich & Simpson (1978) reported SEP enhancement factors that grew exponentially with Z (or A) for C-Zn at 20–300 MeV nucleon^{-1} in the 1977 September 24 event. As in our analysis, their enhancement factors were derived in an energy regime where the species all exhibited nearly identical power-law spectra.

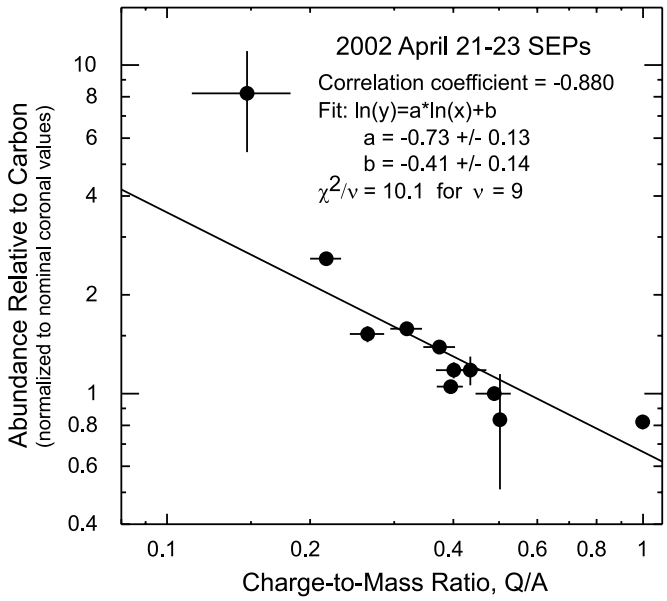

FIG. 11.—Elemental abundances relative to carbon (and normalized to nominal coronal values given by Reames 1995, 2000) vs. charge-to-mass ratio (Q/A), where the charge of $Z > 2$ elements have been taken from the spectral analysis. Also shown is a power-law fit to the correlation.

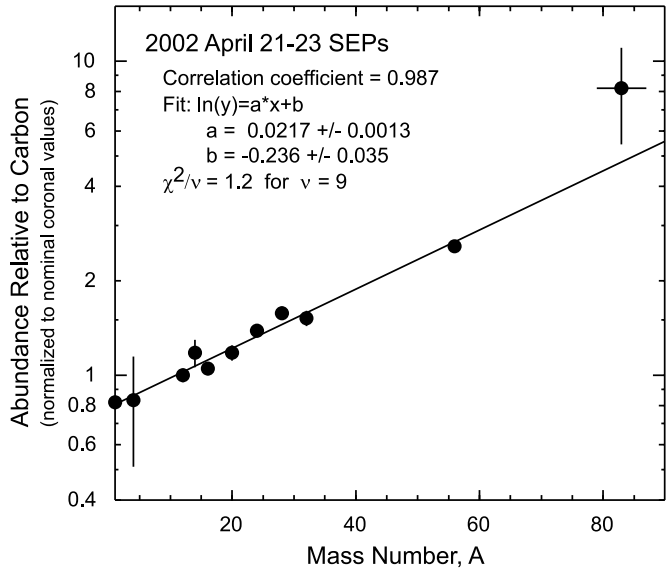

FIG. 12.—Elemental abundances relative to carbon (and normalized to nominal coronal values given by Reames 1995, 2000) vs. mass number A for the 2002 April 21 SEP event. Also shown is an exponential fit to the correlation.

where E and E_{0X} are in units of MeV nucleon^{-1}. This Band et al. function is identical to the Ellison & Ramaty form below the transition energy $(\gamma_{bX} - \gamma_{aX})E_{0X}$, but it is crafted so as to roll smoothly into another power law with no discontinuity in either the function or its first derivative. The Band et al. function was first applied to SEP data in Tylka et al. (2005). Mewaldt et al. (2005) have recently used it in fitting spectra in the large SEP events of 2003 October–November.

The fitted values of the parameters γ_{aX}, γ_{bX}, and E_{0X} are noted in each panel of Figure 13. Also noted are the reduced χ^2 values of the fits, which are on the order of 1–2 for ~20 degrees of freedom. As in Figure 7, χ^2 is evaluated using 15% systematic uncertainty added in quadrature with the statistical errors. The rms deviations of residuals from the fits are typically ~25%. The quality of the fits is slightly poorer here than in Figure 7, but nevertheless acceptable given the somewhat larger instrument-to-instrument normalization discrepancies in this event.[15]

Since the empirical Band et al. functional form is without physical motivation, we hesitate to interpret the fitted values of its parameters. For the purpose of further discussion, we therefore simply characterize the spectra by fitting to two independent power laws, $E^{-\gamma_{\rm low}}$ at energies below 1 MeV nucleon^{-1} and $E^{-\gamma_{\rm high}}$ at energies above 10 MeV nucleon^{-1}. The low-energy power laws do not fit the data as well as the Band function but nevertheless provide a rough characterization of the spectra. The values of these fitted power-law indices, $\gamma_{\rm low}$ and $\gamma_{\rm high}$, are plotted versus atomic number in Figure 14. The $\gamma_{\rm low}$ values are consistent with a common mean, which is also nearly identical to that observed in the 2002 April 21 event (see Fig. 8). For He through Si, the $\gamma_{\rm high}$ values are nearly the same at ~4. But protons, S, and Fe exhibit significantly smaller $\gamma_{\rm high}$ values, indicating high-energy spectra that are harder than those of the other species.

The high-energy spectral differences among species are the other key observational fact that must be accounted for. In the shock-geometry hypothesis, it is suggested that the difference between Fe and the other heavy ions arises from energy dependence in the elemental composition of the seed population. An alternative hypothesis was first outlined by Eichler (1979), who noted that Fe would naturally develop a harder power-law than other species at a so-called "smoothed shock": since Fe ions have a higher A/Q than other ions, they also have a larger scattering mean free path and would therefore be able to traverse larger distances across the smoothed shock. Fe ions thereby sample a larger compression ratio than other species, which would, in turn, manifest itself as a harder power-law index. Similar spectral differences might also arise at the compressive acceleration regions recently considered by Jokipii et al. (2003).

However, in SEP events in which Fe/O rises with energy, observed Fe charge states above ~30 MeV nucleon^{-1} are high, with $\langle Q_{\rm Fe}\rangle \sim 20$, so that there is relatively little difference between the A/Q values of Fe and O. (See Tylka et al. 2005, Fig. 17.) Consequently, in both the "smoothed shock" and compression region scenarios, it would probably also be necessary to invoke some postacceleration stripping. Moreover, in both of these scenarios, one should probably expect protons (which have the smallest A/Q value and therefore the smallest scattering mean free path) to have the steepest spectrum of all. But in fact, protons actually have a harder high-energy power law than the heavy ions. It is therefore unclear whether smoothed shocks or compressive acceleration regions really can account for the observed high-energy spectral differences.

Figure 15 shows the event-averaged spectrum of $34 \leq Z \leq 40$ ions from *Wind* LEMT in this event. The Band et al. fits in Figure 14 suggest that a power law is the appropriate functional

[15] For example, *ACE* SIS and *Wind* LEMT report the Si intensity in two nearly identical energy intervals, at 9–13 and 9.7–13.6 MeV nucleon^{-1}, respectively. After correcting for the slight difference between the intervals, the event-averaged intensities from these two instruments agree to within 1.6% ± 0.1% in the 2002 April 21 event. But in the 2002 August 24 event, the *ACE* SIS intensity is larger by 30% ± 2%. Similarly, *ACE* ULEIS reports the oxygen intensity in the interval 2.56–5.12 MeV nucleon^{-1}, which is also covered by *Wind* LEMT. In the 2002 April 21 event, the instruments' event-averaged intensities in this interval agree to within 8.8% ± 3.0%. But in the 2002 August 24 event, the *ACE* ULEIS intensity is larger by 21% ± 1%. The origin of these discrepancies has not been determined. But one suspects that differences in lookout directions (see discussion in Tylka 2001) and anisotropies (which are generally larger and longer lasting in smaller events; Reames et al. 2001) may be significant factors.

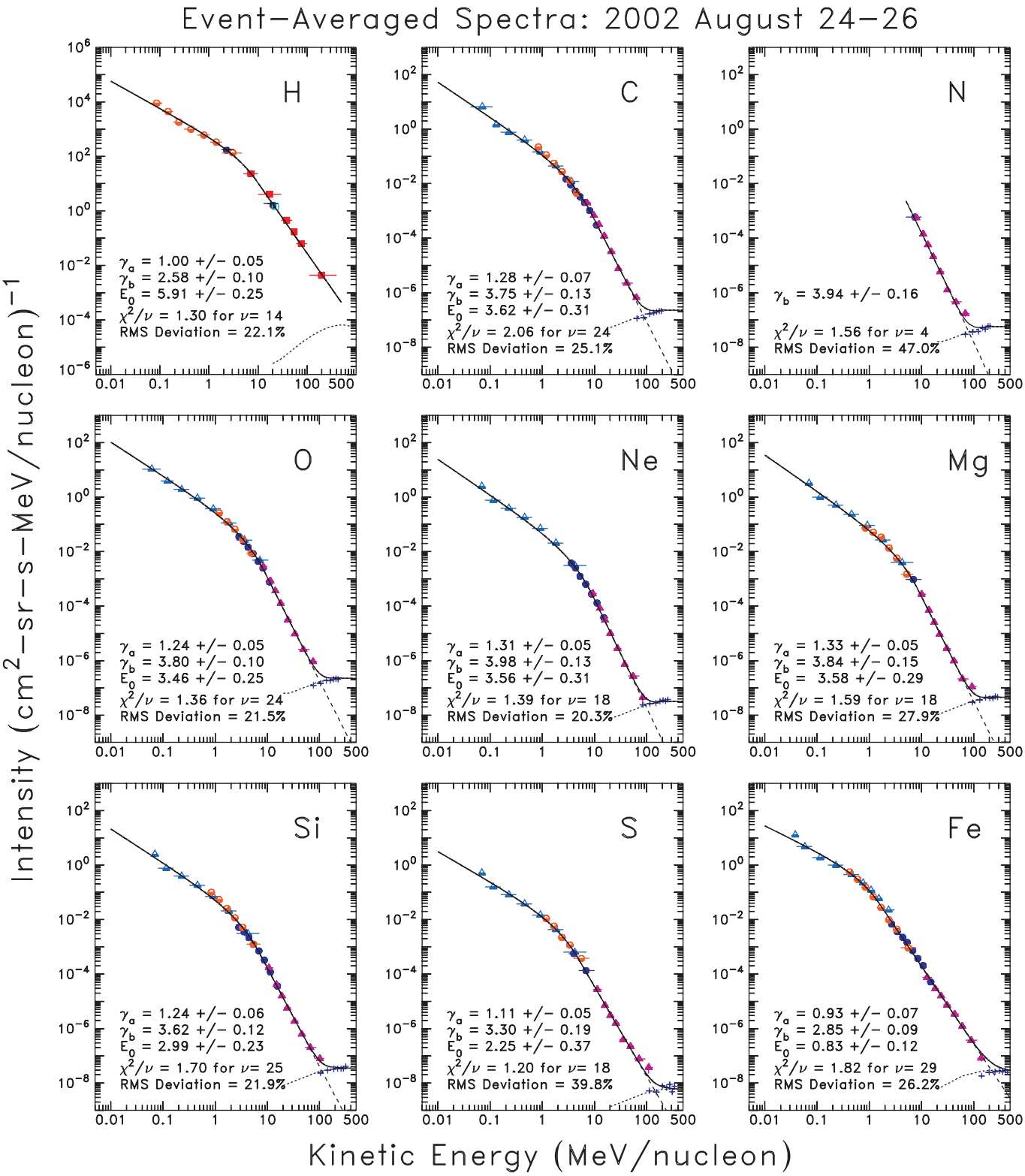

FIG. 13.—Event-averaged spectra for the major elements in the 2002 August 24 solar particle event. The averaging interval began at 0:00 UT on 2002 August 24 and ended at 0:00 UT on 2002 August 27. Instruments are distinguished by color and symbol, as in Fig. 7. Fits are to Band et al. (1993) functions, as described in the text. Fit parameters, reduced χ^2, and rms deviation of the residuals are noted in each panel.

form for these ions in the LEMT energy range. The fitted power law is also shown in Figure 15. Although the error bar is large, the power-law spectrum for the $34 \leq Z \leq 40$ ions (with index $\gamma = 1.97 \pm 0.54$) may be even harder than that of Fe ($\gamma = 2.85 \pm 0.09$).

Finally, we examine the relative elemental composition of the 2002 August 24 event at low energies, where the spectral differences among the species are relatively small. In analogy to Figure 12, we calculated the ratios of normalization coefficients C_X from the power-law fits below 1 MeV nucleon^{-1}. The results

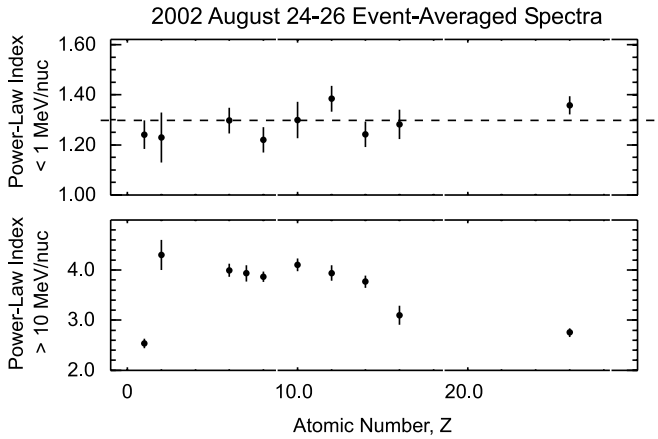

FIG. 14.—Fitted power-law indices below 1 MeV nucleon^{-1} (*top*) and above 10 MeV nucleon^{-1} (*bottom*) vs. atomic number Z for event-averaged energy spectra in the 2002 August 24 event. The dashed line marks the weighted mean of the data points in the top panel.

are plotted versus mass number, A, in Figure 16. As in the 2002 April 21 event, the relative abundances rise exponentially with A. The parameters of the correlation fit in Figure 16 are very similar to those in Figure 12. This comparison emphasizes once again the essential similarity of these two events at low energies.

8. SUMMARY AND DISCUSSION

We have presented details on temporal structure, spectral shapes, and elemental composition in the large, gradual solar energetic particle events of 2002 April 21 and 2002 August 24, supplementing results previously reported in Tylka et al. (2005). These details illustrate, in a relatively clean fashion, the range of phenomenology that SEP modeling efforts must address. Among the differences between the two events, we particularly call attention to the following:

1. *Differences in the temporal dependence of* Fe/O.—Below ~15 MeV nucleon^{-1}, the two events are virtually identical in this regard (see Fig. 4). But at higher energies (Fig. 5), Fe/O falls with increasing energy at all times in the April event. In the August event, on the other hand, Fe/O rises with increasing energy at all times, except perhaps the first 3 hours. These differences in the time-dependent Fe/O are then reflected in the event-averaged results (Fig. 1).

Moreover, in the April event, the fall in Fe/O with increasing energy follows an exponential, with the exponential decay in the first ~8 hr becoming steeper as time goes on.[16] At comparable times in the August event, Fe/O follows a power law in energy, which hardens as time goes on (see Fig. 6).

2. *Differences in the functional forms of the event-averaged energy spectra*.—The event-averaged spectra in the April event are well described by the Ellison & Ramaty (1985) form of a power-law times an exponential, with different e-folding energies for the various species (Figs. 7 and 8). The August event, on the other hand, does not exhibit the exponential, at least not at energies accessible to current instrumentation. Instead, one power law smoothly transitions into a steeper power law, in a way characterized reasonably well by the Band et al. (1993) functional form (Fig. 13). In the August event, the species differ both in the energies at which the transition occurs and in their power-law indices at high energies (Fig. 14). As shown in Tylka et al. (2005), comparable differences between the two events are also apparent in the time-dependent spectra.

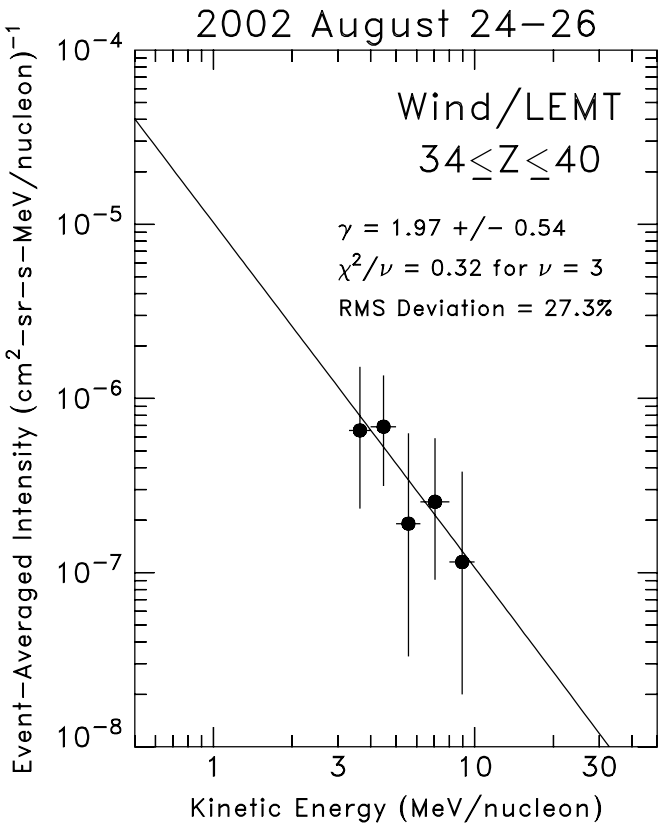

FIG. 15.—Event-averaged spectrum of ions with atomic number $34 \leq Z \leq 40$ from *Wind* LEMT in the 2002 August 24 event and a power-law fit. Data points are plotted with 1 σ Poisson error bars (Gehrels 1986).

3. *Differences in ionic charge states*.—In the 2002 April 21 event, *SAMPEX* has reported $\langle Q_{\rm O} \rangle = 6.3 \pm 0.4$ above ~25 MeV nucleon^{-1}. By comparing spectral shapes (Figs. 7, 8, and 9), we have inferred the mean ionic charges of other species, yielding $\langle Q_{\rm Fe} \rangle = 12.1 \pm 0.9$ and values for other species that are similarly consistent with a common temperature of 1.4 ± 0.1 MK. The time dependence of Fe/O in Figures 4 and 5 is also qualitatively consistent with what would be expected from transport when iron has a significantly smaller charge-to-mass ratio than oxygen.

Unfortunately, we have only limited direct charge-state measurements in the 2002 April 21 event. But a slightly larger event on 2001 September 24 exhibited high-energy spectral shapes and energy-dependent Fe/O very similar to those of 2002 April 21. In the 2001 September 24 event, *SAMPEX* measured $\langle Q_{\rm Fe} \rangle = 10.2 \pm 2.0$ and $\langle Q_{\rm O} \rangle = 6.3 \pm 0.4$ above ~25 MeV nucleon^{-1} (Labrador et al. 2003; A. Labrador 2003, private communication). To within measurement uncertainties, these values are the same as those of the April event. Moreover, the charge states in the 2001 September 24 event were also measured indirectly with the same spectral technique employed in this paper. These indirect measurements agreed with the *SAMPEX* results to within error bars (see Tylka et al. 2005, Fig. 17).

In the 2001 September 24 event, the charge states were also independent of energy to within measurement uncertainties, with $\langle Q_{\rm Fe} \rangle = 10.35 \pm 0.51$ at 0.25–0.50 MeV nucleon^{-1} and

[16] In a survey of traveling interplanetary shocks near Earth in which Fe/O decreased with increasing energy, Tylka et al. (2005) found an anticorrelation, by which the drop-off grew steeper when the measured shock-normal angle $\theta_{\rm Bn}$ was smaller. See Tylka et al. (2005, Fig. 5).

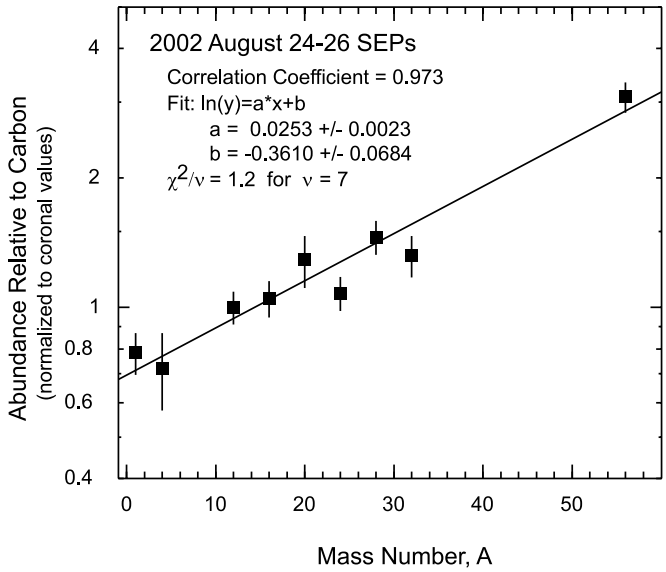

FIG. 16.—Elemental abundances relative to carbon (and normalized to nominal coronal values given by Reames 1995) vs. mass number A for the 2002 August 24 SEP event. Also shown is an exponential fit to the correlation.

$\langle Q_{\rm O}\rangle = 6.73 \pm 0.46$ at 0.5–1.0 MeV nucleon^{-1}. (Mazur & Mason 2001; J. Mazur 2004, private communication). Given the similarities in the others facets of the SEP data, it is reasonable to infer that the 2002 April 21 event, like the 2001 September 24 event, also had little energy dependence in its charge states. Such charge states would also be consistent with the qualitative similarity among the time-dependent Fe/O profiles at various energies (Figs. 4 and 5).

By contrast, the time dependence of Fe/O in the 2002 August 24 event suggests that $\langle Q_{\rm Fe}\rangle$ grows significantly with increasing energy, so that Fe and O have similar charge-to-mass ratios at the highest observed energies. We have no direct measurements of charge states in this event. However, the 2001 April 15 event was another, even larger, ground-level event from a source region near the west limb, with the same high-energy spectral and composition characteristics (Tylka et al. 2002). For this event, *SAMPEX* found that the oxygen charge state went from $\langle Q_{\rm O}\rangle = 6.30 \pm 0.25$ at 0.5–1.0 MeV nucleon^{-1} (Mazur & Mason 2001; J. Mazur 2002, private communication) to $\langle Q_{\rm O}\rangle = 8.0 \pm 0.6$ at >20 MeV nucleon^{-1} (Labrador et al. 2003; A. Labrador 2002, private communication). Similarly, the Fe charge state grew from $\langle Q_{\rm Fe}\rangle = 11.06 \pm 0.37$ at 0.25–0.5 MeV nucleon^{-1} to $\langle Q_{\rm Fe}\rangle = 22.1 \pm 2.9$ above $\sim$30 MeV nucleon^{-1}. Indirect measurements (derived by comparing time-intensity profiles of various energies and species; Dietrich & Tylka 2003) also show $\langle Q_{\rm Fe}\rangle$ increasing with energy in the 2001 April 15 event.

It should be noted that the relative simplicity of the 2002 April 21 event, with its clear exponential rollovers and comparatively low charge states with little energy dependence, consistent with a common source temperature for all species, is rare. Among the 44 large events cataloged in Tylka et al. (2005), we have found only four that clearly exhibit this behavior: 1998 April 20, with source region at W90° and a CME speed[17] of 1863 km s^{-1}; 2000 November 8 at W74° and 1738 km s^{-1}; 2001 September 24 at E23° and 2402 km s^{-1}; and 2002 April 21 at W84° and 2409 km s^{-1}. Thus, conditions that produce this distinctive event type arise only infrequently near the Sun, where the highest energy SEPs are preferentially generated. Nevertheless, this type of event must also be accounted for in SEP modeling. [In modeling the shock-geometry hypothesis (Tylka & Lee 2006), this event type provides the baseline from which more complicated events are generated through parameter variation.]

One might be tempted to think that a variable combination of coronal and flare suprathermals in the shock's seed population might in itself be sufficient to account for the differences between the two events we have been considering here. However, these two events also differ in their spectral character, even for protons and for carbon and oxygen, where there is little room for event-to-event variation in the charge-to-mass ratio. More generally, there is a clear correlation between high-energy Fe/O and spectral shape in large SEP events. (See Tylka et al. 2005, Fig. 9.) The spectral variability indicates that some other factor(s)—in addition to available seed populations—must also be coming into play.

Finally, we also call attention to the striking fractionation pattern (Figs. 12 and 16), below $\sim$1 MeV nucleon^{-1}, where the spectral differences among the species are small. We know of no theoretical explanation for this apparent exponential increase in relative abundance with mass number. Whatever the explanation may be, it apparently operates in the same way in both of these events.

We thank Ilya Usoskin and Eduard Vashenyuk for the Apatity neutron monitor data. We thank Cliff Lopate for making the *IMP-8* CRNE data available to us. We thank Ed Cliver for informative discussions on the solar and radio observations in these events. We thank Gerry Share for providing the *RHESSI* and *Wind* Konus data. This study benefitted from discussions at SHINE meetings (sponsored by NSF, NASA, and AFOSR), which highlighted 2002 April 21 and 2002 August 24 as campaign events. A. J. T. was supported by NASA DPR NNH05AB581 and the Office of Naval Research. W. F. D. was supported under NASA DPR S13823G. M. A. L. was supported by NSF grant ATM-0091527, NASA grant NNG05GL40G, and DoD MURI grants to the University of Michigan and the University of California at Berkeley. C. K. N. was supported under NASA proposal LWS04-0000-0076.

Facilities: ACE (EPAM, SIS, ULEIS), GOES, RHESSI, SAMPEX, SOHO (ERNE, LASCO), WIND (EPACT, KONUS, LEMT, WAVES)

[17] CME speeds were provided by http://cdaw.gsfc.nasa.gov/CME_list/ (Yashiro et al. 2004). The catalog's speed for the 2000 November 8 CME has been revised from previously reported values (Gopalswamy 2003; Tylka et al. 2005).

APPENDIX

TECHNICAL DETAILS OF THE DATA SELECTION AND SPECTRAL FITTING PROCEDURES

Fit parameters and their uncertainties for the Ellison & Ramaty (1985) function were derived by analytically minimizing χ^2. For the Band et al. (1993) function fits, a slightly more complicated procedure was employed. We first did analytic χ^2 minimization to determine two independent power-law fits, one at <1 MeV nucleon^{-1} and the other at >10 MeV nucleon^{-1}. With these results as initial guesses, we performed a grid search of parameter space to find the minimum χ^2 for the Band et al. function fit to the whole

spectrum. We estimated the 1 σ error bar on each Band et al. parameter by examining the changes in χ^2, while that parameter was varied and the others were held constant at their best-fit values.

One other complication in the fitting procedure should be noted. The observed intensities are reported as averages over finite-width energy bins. Consequently, when fitting, the intensity value should be assigned to an abscissa determined by the mean value theorem (MVT). If this is not done and the intensity is instead assigned to the midpoint of the energy interval, the derived spectral parameters will be too hard, especially at high energies, where the energy bins are widest. In our fitting, we used an iterative procedure to address this issue. In a first pass fit, we used the bins' arithmetic midpoints as the abscissae. We then applied the MVT to the fitted function, reevaluated the abscissae, and repeated the fit. This procedure was iterated several times, reevaluating the absicissae after each iteration. After a few iterations, no significant change in χ^2 was observed, and the fit was deemed complete. Throughout this paper, intensity measurements are plotted at abscissae determined by application of the MVT to the fitted functional forms.

With regard to data selection for the spectral analyses, proton measurements below 5 MeV come from *ACE* EPAM, with an additional data point at 2.1–2.3 MeV from *Wind* LEMT. Proton measurements above 5 MeV come primarily from *GOES-8*. The *GOES-8* proton intensities in Figures 7 and 13 were derived by differencing the integral rates at >5, >10, >30, >60, and >100 MeV. We also used the *GOES-8* P7 differential channel, but with an energy interval of 110–400 MeV, as suggested by Smart & Shea (1999). We also included a *SAMPEX* proton measurement at 19–27 MeV (shown as an open square in Figs. 7 and 13).[18] In the August event, which was smaller and caused no apparent saturation problems, we were also able to use a proton measurement at 18.9–21.9 MeV from the APE-B telescope in the *Wind* EPACT instrument package (von Rosenvinge et al. 1995) and a few proton measurements by the Energetic Particle Experiment (ERNE; Torsti et al. 1995; Fig. 13, *black crosses*) on the *Solar and Heliospheric Observatory* (*SOHO*).[19] For the purposes of evaluating χ^2, we assigned total error bars to the proton measurements as 25% for *GOES*; 20% for *SAMPEX*, *SOHO* ERNE, and *Wind* APE-B; and 15% to *ACE* EPAM and *Wind* LEMT.

The *ACE* Science center[20] provided the *ACE* particle data used in this study, except for EPAM $Z \geq 2$ data, which were contributed by one of us (C. G. M.). *ACE* EPAM nitrogen and neon data were not available. *ACE* ULEIS Level-2 data from the *ACE* Science Center do not include nitrogen. Also, as reported there, *ACE* ULEIS results for the elements Ne-S are combined. For the purposes of the spectral studies in Figures 7 and 13, we apportioned the observed ions among the individual elements according to the nominal relative abundances given by Reames (1995). This estimate is considered reliable, since there is little event-to-event variability in the relative abundances within this group of elements, at least below a few MeV nucleon^{-1}. In any case, *ACE* EPAM and *Wind* LEMT measurements overlap the *ACE* ULEIS energy range and provide a check on the results. However, as a result of this procedure, the low-energy spectral parameters for Ne, Mg, Si, and S are not completely independent.

Figures 7 and 13 contain 418 SEP data points. Fifteen data points (not shown) were removed from the analysis because of apparently large systematic errors. All of the removed data points were at the lower edge of an instrument's energy range, where backgrounds and uncertainties in the acceptance are sometimes more acute. For example, *ACE* SIS reports its lowest-energy carbon measurement at 6.1–8.6 MeV nucleon^{-1}. In the August event, this measurement agrees well with measurements from other instruments at nearby and overlapping energies. But in the April event, in which intensities are much higher and background contamination is potentially larger, this particular measurement is higher than those of other instruments by about a factor of 2. In fact, although there are 28 other data points in the carbon spectrum, this single datum alone contributed ~20% of the χ^2. We therefore omitted this particular measurement from our analysis of the April event.

[18] Available from http://cdaweb.gsfc.nasa.gov/cdaweb.
[19] From http://www.srl.utu.fi/projects/erne.
[20] See http://www.srl.caltech.edu/ACE/.

REFERENCES

Aptekar, R. L., et al. 1995, Space Sci. Rev., 71, 265
Arnaud, M., & Raymond, J. 1992, ApJ, 398, 394
Arnaud, M., & Rothenflug, R. 1985, A&AS, 60, 425
Band, D., et al. 1993, ApJ, 413, 281
Bieber, J. W., et al. 2002, ApJ, 567, 622
———. 2004, ApJ, 601, L103
Bougeret, J. L., et al. 1995, Space Sci. Rev., 71, 231
Brenneman, H. H., & Stone, E. C. 1985, ApJ, 299, L57
Brueckner, G. E., et al. 1995, Sol. Phys., 162, 357
Cane, H. V., Erickson, W. C., & Presage, N. P. 2002, J. Geophys. Res., 107, 1315
Cane, H. V., Reames, D. V., & von Rosenvinge, T. T. 1988, J. Geophys. Res., 93, 9555
Cane, H. V., & Richardson, I. G. 2003, J. Geophys. Res., 104, 1156
Cook, W. R. et al. 1993, IEEE Trans. Geosci. Remote Sensing, 31, 557
Dietrich, W. F., & Simpson, J. A. 1978, ApJ, 225, L41
Dietrich, W. F., & Tylka, A. J. 2003, Proc. 28th Int. Cosmic-Ray Conf. (Tsukuba), 6, 3291
Eichler, D. 1979, ApJ, 229, 419
Ellison, D., & Ramaty, R. 1985, ApJ, 298, 400
Garcia-Munoz, M., Mason, G. M., & Simpson, J. A. 1975, ApJ, 201, L145
Gehrels, N. 1986, ApJ, 303, 336
Gold, R. E., et al. 1998, Space Sci. Rev., 86, 541
Gopalswamy, N. 2003, Geophys. Res. Lett., 30, 8013
Gopalswamy, N., Yashiro, S., Krucker, S., Stenborg, G., & Howard, R. A. 2004, J. Geophys. Res., 109, A12105
Jokipii, J. R. 1987, ApJ, 313, 842
Jokipii, J. R., Giacalone, J., & Kóta, J. 2003, Proc. 28th Int. Cosmic-Ray Conf. (Tsukuba), 6, 3685
Kahler, S. W. 2001, J. Geophys. Res., 106, 20947
Klein, K.-L., & Posner, A. 2005, A&A, 438, 1029
Kocharov, L., Lytova, M., Vainio, R., Laitenen, T., & Torsti, J. 2005, ApJ, 620, 1052
Kocharov, L., & Torsti, J. 2003, ApJ, 586, 1430
Labrador, A. W., Leske, R. A., Mewaldt, R. A., Stone, E. C., & von Rosenvinge, T. T. 2003, Proc. 28th Int. Cosmic-Ray Conf. (Tsukuba), 6, 3269
Lee, M. A. 2005, ApJS, 158, 38
Leske, R. A., et al. 2003, Proc. 28th Int. Cosmic-Ray Conf. (Tsukuba), 6, 3253
Li, G., & Zank, G. P. 2005, Geophys. Res. Lett., 32, 02101
Li, G., Zank, G. P., & Rice, W. K. M. 2003, J. Geophys. Res., 108, 1082
Lin, R. P., et al. 2002, Sol. Phys., 210, 3
Lintunen, J., & Vainio, R. 2004, A&A, 420, 343
Mason, G. M., et al. 1998, Space Sci. Rev., 86, 409
Mazur, J. E., & Mason, G. M. 2001, Eos Trans. AGU, 82(47), Fall Meet. Suppl. Abstract SH31C-03
Mewaldt, R. A., et al. 2005, J. Geophys. Res., 110, 09S18
Miroshnichenko, L. I., Klein, K.-L., Trottet, G., Lantos, P., Vashenyuk, E. V., & Balabin, Yu.V. 2005, Adv. Space Res., 35, 1864
Ng, C. K., Reames, D. V., & Tylka, A. J. 1999, Geophys. Res. Lett., 26, 2145
———. 2003, ApJ, 591, 461
Ogilvie, K., et al. 1995, Space Sci. Rev., 71, 55
Parker, E. N. 1963, Interplanetary Dynamical Processes (New York: Interscience Publ.)

Post, D. E., Jensen, R. V., Tarter, C. B., Grasberger, W. H., & Lokke, W. A. 1977, At. Data Nucl. Data Tables, 20, 397
Reames, D. V. 1995, Adv. Space Res., 15(7), 41
———. 2000, ApJ, 540, L111
Reames, D. V., Barbier, L. M., & Ng, C. K. 1996, ApJ, 466, 473
Reames, D. V., Meyer, J. P., & von Rosenvinge, T. T. 1994, ApJS, 90, 649
Reames, D. V., & Ng, C. K. 2004, ApJ, 610, 510
Reames, D. V., Ng, C. K., & Berdichevsky, D. 2001, ApJ, 550, 1064
Rice, W. K. M., Zank, G. P., & Li, G. 2003, J. Geophys. Res., 108, 1369
Richardson, I. G., & Cane, H. V. 1996, J. Geophys. Res., 101, 27521
Roussev, I. I., et al. 2004, ApJ, 605, L73
Ruffolo, D., et al. 2006, ApJ, 639, 1186
Sáiz, A., et al. 2005, ApJ, 626, 1131
Smart, D. F., & Shea, M. A. 1999, Radiat. Measurements, 30, 327
Sokolov, I. V., et al. 2004, ApJ, 616, L171
Stone, E. C., et al. 1998a, Space Sci. Rev., 86, 357
Stone, E. C., et al. 1998b, Space Sci. Rev., 86, 285
Torsti, J., et al. 1995, Sol. Phys., 162, 505
Tylka, A. J. 2001, J. Geophys. Res., 106, 25333
Tylka, A. J., Boberg, P. R., McGuire, R. E., Ng, C. K., & Reames, D. V. 2000, in AIP Conf. Proc. 528, Acceleration and Transport of Energetic Particles in the Heliosphere, ed. R. A. Mewaldt, J. R. Jokipii, M. A. Lee, E. Möbius, & T. H. Zurbuchen (Melville: AIP), 147
Tylka, A. J., & Lee, M. A. 2006, ApJ, in press
Tylka, A. J., et al. 2002, ApJ, 581, L119
———. 2003, Proc. 28th Int. Cosmic-Ray Conf. (Tsukuba), 6, 3305
———. 2005, ApJ, 625, 474
von Rosenvinge, T. T., et al. 1995, Space Sci. Rev., 71, 155
Webb, G. M., Zank, G. P., Ko, C. M., & Donohue, D. J. 1995, ApJ, 453, 178
Yashiro, S., et al. 2004, J. Geophys. Res., 109, 07105
Zank, G. P., Rice, W. K. M., & Wu, C. C. 2000, J. Geophys. Res., 105, 25079